IN-14291

NASA Technical Memorandum 87675

TIME-DEPENDENT SOLUTION FOR AXISYMMETRIC FLOW OVER A BLUNT BODY WITH IDEAL GAS, CF_4, OR EQUILIBRIUM AIR CHEMISTRY

H. Harris Hamilton II and

John R. Spall

July 1986

National Aeronautics and Space Administration

Langley Research Center
Hampton, Virginia 23665

TIME-DEPENDENT SOLUTION FOR AXISYMMETRIC FLOW OVER A BLUNT BODY WITH IDEAL GAS, CF_4, OR EQUILIBRIUM AIR CHEMISTRY

H. Harris Hamilton II

and

John R. Spall

INTRODUCTION

Over the past three decades, much effort has been devoted to solving the inviscid flow over blunt bodies. Two basic approaches have been used: (1) an inverse approach - where the shock wave is given and the body shape and details of the flow within the shock layer are unknown and (2) a direct approach - where the body shape is given and all details of the flow within the shock layer are unknown. (See ref. 1.)

For the inverse problem, the steady flow equations are usually solved by marching inward from the shock wave to obtain the solution for the body. (See refs. 2 to 5.) Since the steady flow equations are of a mixed elliptic-hyperbolic type, this initial value problem is ill posed and is inherently unstable. However, for some cases good results can be obtained by this approach before the instabilities destroy the solution (refs. 1 and 2). The inverse problem can be made direct by iteration. However, improvements to a solution which gives an approximation to a desired body shape is not always apparent (ref.1), and thus solutions for complex body shapes are usually difficult to obtain.

More recently, time-dependent, finite-difference techniques have been used with great success to solve the more difficult direct problem. (See refs. 6 to 11). This technique takes advantage of the hyperbolic nature of the unsteady flow equations by marching in time from an approximate initial condition to the desired steady-state solution. This problem is well posed and thus eliminates the instabilities that were mentioned earlier for the inverse problem. This technique has been used successfully to compute the flow over very complex geometries.

The purpose of the present paper is to describe such a time-dependent, finite-difference computer code, developed by the senior author, which has been used successfully for the past several years to analyze inviscid flow fields over axisymmetric bodies at zero degrees angle of attack. The code has the capability of calculating the flow of an ideal gas, CF_4, or air in chemical equilibrium and can be applied to reasonably general axisymmetric body shapes. The present paper gives a detailed description of the method

of solution and presents some comparisons of calculated results with experimental data.

SYMBOLS

a	speed of sound, $\bar{a}/\bar{V}_\infty$
B_b	body bluntness parameter
c_p	specific heat at constant pressure
c_v	specific heat at constant volume
g, g_1	parameters defined by equations (16)
H	total enthalpy, $\bar{H}/\bar{V}_\infty^2$
h	static enthalpy, $\bar{h}/\bar{V}_\infty^2$
j	indicator, j=0 for 2-D flow, j=1 for axisymmetric flow
M	Mach number
p	pressure, $\bar{p}/\bar{\rho}_\infty\bar{V}_\infty^2$
r, ϕ	polar coordinates (See fig. 1.)
$\bar{R}$	gas constant for CF_4, 94.475 J/kg-K
$\bar{R}_b$	radius of curvature of nose, m
t	time, $\bar{V}_\infty\bar{t}/\bar{R}_b$
$\bar{t}$	dimensional time, sec
V_∞	free-stream velocity, $\bar{V}_\infty/\bar{V}_\infty = 1$
$\bar{V}_\infty$	dimensional free-stream velocity, m/sec

$(v_n)_s$ velocity component normal to shock wave, $(\bar{v}_n)_s/\bar{V}_\infty$

v_r, v_ϕ velocity components in polar coordinate system (see fig. 1), $\bar{v}_r/\bar{V}_\infty$ and $\bar{v}_\phi/\bar{V}_\infty$

x, y Cartesian coordinates (see fig. 3), $\bar{x}/\bar{R}_b$, $\bar{y}/\bar{R}_b$

x_p location of pole of coordinate system (see fig. 3), $\bar{x}_p/\bar{R}_b$

β_s shock wave angle

δ normal distance between body and shock, m

γ ratio of specific heats, $\bar{c}_p/\bar{c}_v$

Δr local shock layer thickness in radial direction (eq.(12c))

$\Delta\eta$ step size in η-direction

$\Delta\xi$ step size in ξ-direction

ε artificial viscosity

ζ_b angle between tangent to body and line r = Constant

ζ_s angle between tangent to shock and line r = Constant

η_r, η_ϕ derivative of η with respect to r and ϕ (eqs.(12a) and (12d))

ξ, η transformed coordinates defined by equations (9) and (10)

ξ_r, ξ_ϕ derivatives of ξ with respect to r and ϕ (eqs. (12b) and (12e))

ρ density, $\bar{\rho}/\bar{\rho}_\infty$

Superscripts:

$(\bar{\ })$ dimensional quantity

$(\hat{\ })$ predicted quantity

Subscripts:

b body

s	shock
w	wall
∞	free stream
max	maximum

METHOD

This section presents a description of the time-dependent, finite-difference technique used to solve the inviscid two-dimensional or axisymmetric flow over a blunt-nosed body such as that shown in figure 1. The domain of the solution includes the entire subsonic portion of the flow field with the downstream outflow boundary located in a region where the flow is completely supersonic.

Flow-Field Equations

The partial differential equations governing the two-dimensional or axisymmetric flow of an inviscid, nonconducting fluid in polar coordinates (fig. 1) are

$$\frac{D\rho}{Dt} = \rho\left(\frac{\partial v_r}{\partial r} + \frac{1}{r}\frac{\partial v_\phi}{\partial \phi} + \frac{j-1}{r}v_r + j\frac{\cot\phi}{r}v_r\right) \tag{1}$$

$$\frac{Dv_r}{Dt} - \frac{v_\phi^2}{r} + \frac{1}{\rho}\frac{\partial p}{\partial r} = 0 \tag{2}$$

$$\frac{Dv_\phi}{Dt} + \frac{v_r v_\phi}{r} + \frac{1}{r\rho}\frac{\partial p}{\partial \phi} = 0 \tag{3}$$

where

$$\frac{D}{Dt} = \frac{\partial}{\partial t} + v_r\frac{\partial}{\partial r} + \frac{v_\phi}{r}\frac{\partial}{\partial \phi}$$

denotes the substantial derivative and j=0 for two-dimensional flow and j=1 for axisymmetric flow.

Since entropy is constant along streamlines, the following relation can be written between pressure and density:

$$\frac{Dp}{Dt} = a^2 \frac{D\rho}{Dt} \tag{4}$$

which can be used in the continuity equation (1) to replace the density derivative to obtain the following equation:

$$\frac{Dp}{Dt} + a^2\rho\left(\frac{\partial v_r}{\partial r} + \frac{1}{r}\frac{\partial v_\phi}{\partial \phi} + \frac{j+1}{r} v_r + j \frac{\cot\phi}{r} v_\phi\right) \tag{5}$$

Now equations (2), (3), and (5) contain derivatives of p, v_r, and v_ϕ only and are in a convenient form to solve for these variables. One other equation is needed to solve for a second thermodynamic variable. Since our interest is only in the steady flow solution, the integrated form of the energy equation is used

$$H = h + \frac{v_r^2 + v_\phi^2}{2} \tag{6}$$

Although this will cause the time-varying solution to be inconsistent, it will yield consistent and accurate steady-state results. Now equations (2), (3), (5), and (6) contain six dependent variables (p, ρ, a, v_r, v_ϕ, and h). To solve for these variables, two additional equations are needed. These can be obtained from the thermodynamic equation of state in the following functional form:

$$\rho = \rho(p,h) \tag{7}$$

$$a = a(p,h) \tag{8}$$

The method of computing these properties for different gases will be discussed in the section on thermodynamic properties.

Computational Domain

To make integration of this system of partial differential equations easier and to help with the application of boundary conditions, the region (fig. 1) bounded by the stagnation streamline, the bow shock wave, a line $\phi = \phi_{max}$ (located in the supersonic flow region), and the body surface is mapped into a rectangular domain (fig. 2) using the transformation equations

$$\xi = \frac{\phi}{\phi_{max}} \tag{9}$$

$$\eta = \frac{r - r_b(\phi)}{r_s(\phi) - r_b(\phi)} \tag{10}$$

From these transformation equations, a set of transformation operators can be defined as

$$\frac{\partial}{\partial r} = \eta_r \frac{\partial}{\partial \eta} + \xi_r \frac{\partial}{\partial \xi} \tag{11a}$$

$$\frac{\partial}{\partial \phi} = \eta_\phi \frac{\partial}{\partial \eta} + \xi_\phi \frac{\partial}{\partial \xi} \tag{11b}$$

where

$$\eta_r = \frac{1}{\Delta r} \tag{12a}$$

$$\xi_r = 0 \tag{12b}$$

$$\Delta r = r_s(\phi) - r_b(\phi) \tag{12c}$$

$$\eta_\phi = -\frac{1}{\Delta r}\left(\frac{dr_b}{d\phi} + \frac{d(\Delta r)}{d\phi}\right) \tag{12d}$$

$$\xi_\phi = \frac{d\xi}{d\phi} = \frac{1}{\phi_{max}} \tag{12e}$$

which will transform the governing partial differential equations (2), (3) and (5) into the following system

$$\frac{\partial p}{\partial t} = -g \frac{\partial p}{\partial \eta} - g_1 \frac{\partial p}{\partial \xi} - a^2 \rho \left(\frac{1}{\Delta r} \frac{\partial v_r}{\partial \eta} + \frac{1}{r}\left(\xi_\phi \frac{\partial v_\phi}{\partial \xi} + \eta_\phi \frac{\partial v_\phi}{\partial \eta}\right)\right.$$

$$+ \frac{v_r}{r}(j+1) + j\frac{\cot\phi}{r} v_\phi) \tag{13}$$

$$\frac{\partial v_r}{\partial t} = -\left(g\frac{\partial v_r}{\partial \eta} + g_1\frac{\partial v_r}{\partial \xi} - \frac{v_\phi^2}{r} + \frac{1}{\rho\Delta r}\frac{\partial p}{\partial \eta}\right) \tag{14}$$

$$\frac{\partial v_\phi}{\partial t} = -\left(g\frac{\partial v_\phi}{\partial \eta} + g_1\frac{\partial v_\phi}{\partial \xi} + \frac{v_r v_\phi}{r} + \frac{1}{\rho r}\left(\xi_r\frac{\partial p}{\partial \xi} + \eta_\phi\frac{\partial p}{\partial \eta}\right)\right) \tag{15}$$

where

$$g = \frac{v_r}{\Delta r} + v_\phi\left(\frac{\eta_\phi}{r}\right) \tag{16a}$$

$$g_1 = v_\phi\left(\frac{\xi_\phi}{r}\right) \tag{16b}$$

Numerical Procedure

Interior grid points.- At all interior grid points, the governing differential equations (eqs. (13) to (15)) are integrated in time, using the Brailovskaya difference scheme (ref. 12). This same technique has been used by Barnwell (ref. 9) for invisicd flow calculations and Carter (ref. 13) for viscous flow calculations. It is an explicit, predictor-corrector technique which uses forward time and centered spatial derivatives.

When it is applied to a general partial differential equation of the form

$$\frac{\partial f}{\partial t} + f\frac{\partial f}{\partial x} = 0 \tag{17a}$$

it yields the following result:

Predictor step:

$$\hat{f}_i^{n+1} = f_i^n - \frac{\Delta t}{2\Delta x} f_i^n\left(f_{i+1}^n - f_{i-1}^n\right) \tag{17b}$$

Corrector step:

$$f_i^{n+1} = f_i^n - \frac{\Delta t}{2\Delta x} \hat{f}_i^n (\hat{f}_{i-1}^{n-1} - \hat{f}_{i+1}^{n+1}) \tag{17c}$$

where n indicates the time step and i indicates the spatial grid point.

Differencing at the boundaries.- At the shock, body surface, and outflow boundaries, three-point, one-sided differences are used for the spatial derivatives in a direction normal to the boundary (see fig. 2) in both the predictor and corrector steps. Thus, the same order accuracy is maintained at the boundaries as at the interior points. Symmetry conditions are applied along the stagnation streamline.

Shock-wave solution.- A method similar to that used by Hamilton and Graves (ref. 10) has been used to track the movement of the shock wave during the transient portion of the solution. The method can be summarized as follows. (Details are given in the appendix.) First, the pressure is computed on the downstream of the shock wave by using the two-step difference scheme described previously. With the pressure at the shock wave p_s known, the density is computed for an ideal gas from the equation

$$\frac{1}{\rho_s} = \frac{h_\infty + \frac{1}{2}(p_s - p_\infty)}{p_s(\frac{\gamma}{\gamma-1}) - \frac{1}{2}(p_s - p_\infty)} \tag{18}$$

and then the shock velocity is computed from the equation

$$v_s = (v_n)_\infty - \left(\frac{p_s - p_\infty}{1 - \frac{1}{\rho_s}}\right)^{1/2} \tag{19}$$

where v_s and $(v_n)_\infty$ are defined in the sketches in the appendix. Next, the movement of the shock wave is computed from the following differential equation:

$$\frac{dr_s}{dt} = -V_s/\cos\zeta_s \tag{20}$$

where

$$\zeta_s = \tan^{-1}\left(\frac{1}{r_s}\frac{\partial r_s}{\partial \phi}\right) = \tan^{-1}\left(\frac{\xi_\phi}{r_s}\frac{\partial r_s}{\partial \xi}\right) \tag{21}$$

by using the following two-step finite difference approximation:

Predictor step:

$$(\hat{r}_s)^{t+\Delta t} = r_s^t + \Delta t(V_s/\cos\zeta_s)^t \tag{22}$$

Corrector step:

$$(r_s)^{t+\Delta t} = r_s^t + 0.5\Delta t((V_s/\cos\zeta_s)^t + (\hat{V}_s/\cos\hat{\zeta}_s)^{t+\Delta t}) \tag{23}$$

For CF_4 and equilibrium air chemistry, the γ used in equation (18) is replaced by γ_ρ. (See section on Thermodynamics.) Thus, for these cases the method of tracking the transient shock wave is approximate during the early part of the solution, but becomes more exact as the steady state is approached.

Derivatives along the shock, $dr_s/d\xi$, are calculated using a noncentered four-point formula of the form

$$\left(\frac{dr_s}{d\xi}\right)_i = \frac{1}{6\Delta\xi}\left(r_{s_{i-2}} - 6r_{s_{i-1}} + 3r_{s_i} + 2r_{s_{i+1}}\right) \tag{24}$$

where i indicates the grid point location. Numerical experimentation has shown that this form of the shock derivative produces a much smoother converged shock than centered differences.

Wall boundary conditions.- For inviscid flow, the velocity must be tangent to the wall (i.e. the normal component of velocity must be zero). This requires that the following equation be satisfied

$$(v_r)_w = (v_\phi)_w(\tan\zeta_b) \tag{25}$$

where

$$\zeta_b = \tan^{-1}\left(\frac{1}{r_b}\frac{\partial r_b}{\partial \phi}\right) = \tan^{-1}\left(\frac{\xi_\phi}{r_b}\frac{\partial r_b}{\partial \xi}\right) \tag{26}$$

The wall boundary condition is applied using the following procedure:

1. The pressure at the wall (p_w) is first determined by integrating equation (13).

2. The "estimated" values for the wall velocity components, $(v_r^*)_w$ and $(v_\phi^*)_w$, are obtained by integrating equations (14) and (15), respectively.

3. The "final" value for the ϕ-component of velocity at the wall, $(v_\phi)_w$, is obtained by combining equation (25) with the expression for total velocity to obtain:

$$(v_\phi)_w = \left((v_r^*)_w^2 + (v_\phi^*)_w^2\right)/(1 + \tan^2\zeta_b))^{1/2} \tag{27}$$

4. The "final" value for the r-component of velocity at the wall, $(v_r)_w$, is then calculated from equation (25).

5. Using these values of velocity, the wall enthalpy, h_w, is calculated from equation (6).

This procedure is applied at the wall in both the predictor and corrector steps of the integration process.

Smoothing function.- Numerical experimentation has shown that the present solution converges much more rapidly and is less likely to diverge for a given set of initial conditions if a small amount of explicit numerical smoothing is applied during the integration. In the present program, the fourth-order smoother of Barnwell (ref. 9) has been used. The smoothing is applied to the dependent variables (p, v_r, and v_ϕ) in equations (13) through (15) during the the corrector step. Small values of the smoothing coefficient of the order of 0.02 are typically used in the results presented in the present paper and have been found adequate to damp out unwanted oscillations without distorting the computed flow field.

Stability.- The flow-field equations are integrated in the present method using the maximun allowable "local" time step at each grid point. This has been found to produce almost identical results as solutions obtained using the minimum "global" time step, but the speed of convergence is "approximately" doubled. To estimate the maximum allowable local time step the following approximate CFL relation is used

$$\Delta t = \frac{(\Delta s)_{min}}{|v_r| + |v_\phi| + a\left(\frac{1}{\Delta r} + \frac{1}{r\Delta\phi}\right)^{1/2}} \tag{28}$$

where $(\Delta s)_{min}$ is the minimum local grid spacing. In actual applications, approximately 50 to 80 percent of the time step calculated from the above equation is used in the integration at each grid point.

Thermodynamics

To compute an actual flow field, density (ρ) and speed of sound (a) must be determined as a function of pressure and enthalpy (p and h). This is expressed in functional form by equations (7) and (8). For an ideal gas, these expressions are simply

$$\rho = \left(\frac{\gamma}{\gamma - 1}\right)\frac{p}{h} \tag{29a}$$

$$a^2 = (\gamma - 1)h \tag{29b}$$

Such simple closed form expressions are not possible for CF_4. For this case, the expressions given by Sutton (ref. 14) have been used to obtain a curve fit of

$$\bar{T} = \bar{T}(\bar{h})$$

over range of temperatures from 100° to 1000° Kelvin. Thus, once h has been computed, $\bar{T}$ can be determined from the above curve fit, and $\bar{\rho}$ can be computed from the thermally perfect equation of state:

$$\bar{p} = \bar{\rho}\bar{R}\bar{T} \tag{30}$$

where $\bar{R}$ is the gas constant for CF_4 (94.465 J/kg-K). The speed of sound (a) can then be determined from the expressions given by Sutton in (ref. 14).

For air in chemical equilibrium, simple closed form expressions for ρ and a^2 are also impossible to obtain. For this case, Kenneth Sutton has developed a set of thermodynamic subroutines based on the approximate approach of Hanson (ref. 15) which yield all of the desired thermodynamic properties for air at high temperatures as a function of pressure and

temperature. To use these subroutines in the present program, an iterative scheme was developed to enable all of the desired thermodynamic properties to be determined as a function of pressure and enthalpy.

However, for both CF_4 and equilibrium air, the computational time is greatly increased above that required for an ideal gas if the thermodynamic routines are called for each time step. Thus a relatively simple procedure has been used which requires calling the thermodynamic subroutines only one time each 25 to 50 time steps. This procedure requires calling the thermodynamic subroutines at the first time step and evaluating the values of γ_ρ and γ_a at each grid point which satisfy the equations:

$$\rho = \left(\frac{\gamma_\rho}{\gamma_\rho - 1}\right)\frac{p}{h} \tag{31}$$

$$a^2 = (\gamma_a - 1)h \tag{32}$$

These values of γ_ρ and γ_a are stored and used in successive time steps to calculate the required values of ρ and a^2 for each integration step. Since the flow-field quanities change slowly, these approximate values of ρ and a^2 are sufficiently accurate to proceed with the solution. At regular intervals, the thermodynamic subroutines are called to up date the values of γ_ρ and γ_a. As the result of several tests, using this procedure requires an update to the thermodynamics every 50 iterations. This reduces much of the computational overhead so that these types of solutions require only 15 to 20 percent more time than an ideal gas solution.

Body Geometry

The forward portion of the body geometries considered in the present paper have a projection in the $\bar{x},\bar{y}$ plane that is described by the equation for a general conic section:

$$\bar{y}^2 = 2\bar{R}_b\bar{x} - B_b\bar{x}^2 \tag{33}$$

where $\bar{R}_b$ is the radius of curvature at the stagnation point (where $\bar{x} = 0$) and B_b is a bluntness parameter. The bluntness parameter B_b characterizes the eccentricity of the conic section. Its significance is

better understood if it is noted that $B_b < 0$ generates a hyperbola, $B_b = 0$ generates a parabola, and $B_b > 0$ generates an ellipse (with $B_b = 1$ for the special case of a circle). For an ellipse, B_b is related to the ratio of the major to minor axes (b/a) by the equation

$$B_b = (b/a)^2 \tag{34}$$

Some of the body shapes considered in the present paper were blunted cones. These shapes can be generated by using equation (33) to describe the nose followed by a straight line segment to describe the remaining downstream segment of the body.

RESULTS AND DISCUSSION

In this section, results of the present method are compared with experimental data and the results of other numerical techniques. Two gases are considered: air with either ideal gas and equilibrium chemistry, and CF_4. Flow over a sphere, a paraboloid, and two different ellipsoids is considered for the ideal gas cases; flow over a sphere-cone for the equilibrium air case; and flow over a sphere for the CF_4 case. For all cases, 41 points are used around the body and 21 points are used between the body and shock.

Air

Surface pressure distributions on a sphere in air for Mach numbers of 2.0, 4.0, and 8.06 and $\gamma = 1.4$ are given in figure 4. To maintain a supersonic outflow boundary condition, Φ_{max} was set equal to 45 degrees for the two higher Mach number cases and 55 degrees for the Mach 2 case. Agreement between the present method and the data of references 2, 5, and 16 is excellent. Shock-layer thicknesses for each Mach number are given in figure 5. Again, there is excellent agreement between the present method and the numerical and experimental data at the higher Mach numbers. However, at a Mach number of 2.0, there is a maximum difference between the present method and the experimental data of reference 16 of 6 percent. As noted in reference 5, the shock-layer thickness changes rapidly at low Mach numbers; and thus, a small error in the test Mach number could be enough to cause this difference in results.

Pressure distributions on a paraboloid for Mach numbers of 3 and 10 and $\gamma = 1.4$ are given in figure 6. The data of the present method are in very good agreement with the numerical results of references 2 and 5 for both Mach numbers. Shock-layer thicknesses are compared in figure 7, and again, agreement is very good.

Surface pressure distributions for ellipsoids with b/a = 0.5 and 1.5 are given in figures 8 and 9 for $\gamma = 1.4$ and Mach numbers of 4.0 and 8.06. Agreement between the present method and the data of references 5 and 16 is excellent. Shock-layer thicknesses for the case where b/a = 1.5 are given in figure 10. Agreement is very good for both Mach numbers.

In figures 11 and 12, surface pressure distributions and shock-layer thicknesses are given for flow over a spherically blunted cone, where equilibrium air chemistry is used. Comparisons are made with the computational data of references 17 and 18. Agreement is generally very good except for the shock-layer thickness for values of $s/R_b > 2.5$, where the present method produces results that are slightly higher than the other data shown.

CF_4

The surface pressure distribution on a sphere in CF_4 is given in figure 13. The computer code described in reference 17 was used to generate the data for comparison. The agreement is excellent. The computed shock standoff distance around the body is shown in figure 14 along with data generated by the code of reference 17. Again, the agreement is excellent.

CONCLUDING REMARKS

A time-asymptotic method has been used to obtain steady-flow solutions for axisymmetric, inviscid flow over several blunt bodies including spheres, paraboloids, ellipsoids, and spherically blunted cones. Comparisons with experimental data and results of other computational methods have demonstrated that accurate solutions can be obtained using this approach. The method should prove useful as an analysis tool for comparing with experimental data and for making engineering calculations for blunt reentry vehicles.

APPENDIX

CALCULATION OF PROPERTIES AT SHOCK WAVE

A method similar to that presented in reference 10 has been used to calculate the shock velocity and other thermodynamic properties at the shock wave from the pressure. Consider the shock wave illustrated in the sketch (a) which can be expressed as a function of ϕ, $r_s = r_s(\phi)$

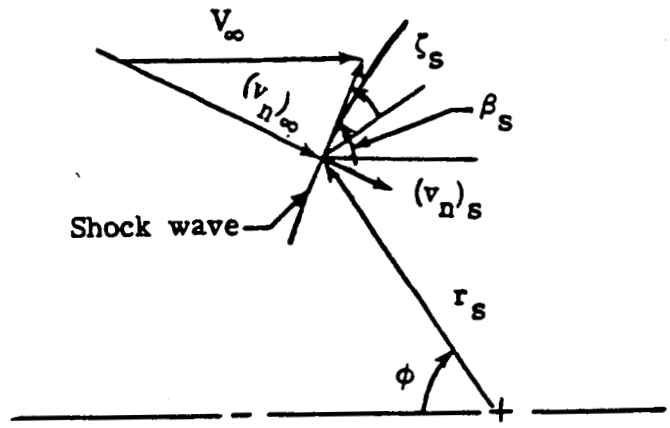

Sketch (a)

The shock-wave angle β_s is given by the equation

$$\beta_s = \frac{\pi}{2} - \phi + \zeta_s \tag{A1}$$

where

$$\zeta_s = \tan^{-1}\left(\frac{1}{r_s}\frac{\partial r_s}{\partial \phi}\right) = \tan^{-1}\left(\frac{\xi_\phi}{r_s}\frac{\partial r_s}{\partial \xi}\right) \tag{A2}$$

and the components of free-stream velocity tangent and normal to the shock wave are given, respectively, by the equations

$$(V_t)_\infty = V_\infty \cos\beta_s \tag{A3}$$

$$(V_n)_\infty = V_\infty \sin\beta_s \tag{A4}$$

Changes in properties across the shock wave can be related to the normal component of free-stream velocity and the shock velocity, as illustrated in sketch (b).

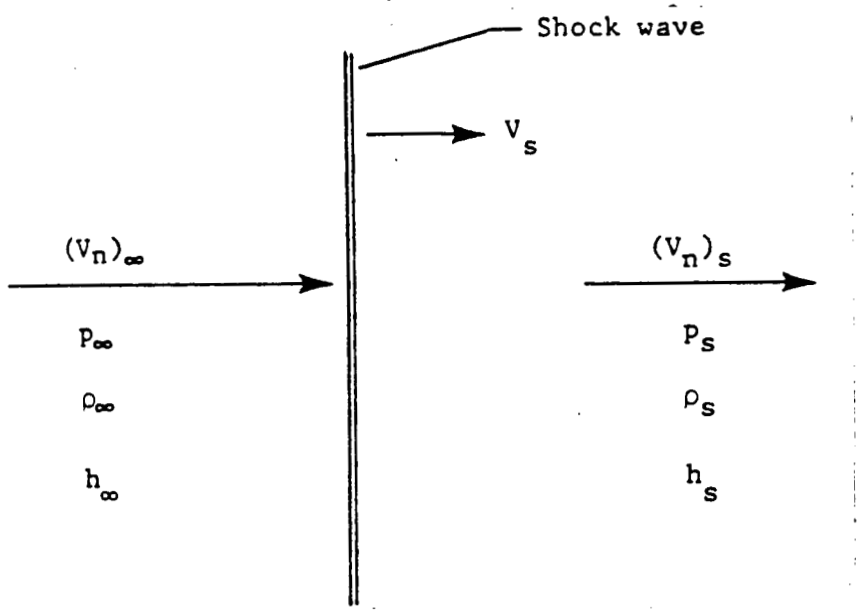

Sketch (b)

Conditions across the shock can be related by the following normal shock-wave equation (since $\rho_\infty = 1$):

$$(V_n)_\infty - V_s = \rho_s[(V_n)_s - V_s] \tag{A5}$$

$$p_\infty + [(V_n)_\infty - V_s]^2 = p_s + [(V_n)_s - V_s]^2 \tag{A6}$$

$$h_\infty + \frac{[(V_n)_\infty - V_s]^2}{2} = h_s + \frac{[(V_n)_s - V_s]^2}{2} \tag{A7}$$

Now rearranging equation (A6), the following expression can be obtained:

$$p_s - p_\infty = [(V_n)_\infty - V_s]^2 \left\{ 1 - \rho_s \frac{[(V_n)_s - V_s]^2}{[(V_n)_\infty - V_s]^2} \right\} \tag{A8}$$

Combining this equation with equation (A5) and solving for $[(V_n)_\infty - V_s]^2$, the following result is obtained

$$[(V_n)_\infty - V_s)]^2 = \frac{p_s - p_\infty}{1 - \frac{1}{\rho_s}} \tag{A9}$$

Similarly, equation (A6) becomes

$$h_s = h_\infty + \frac{1}{2}[(V_n)_\infty - V_s]^2 \left[1 - \frac{1}{\rho_s}\right]^2 \tag{A10}$$

Equations (A9) and (A10) can be combined with the ideal-gas equation of state $p = \rho(\frac{\gamma - 1}{\gamma})h$ to yield the following result:

$$\frac{1}{\rho_s} = \frac{h_\infty + \frac{1}{2}(p_s - p_\infty)}{p_s(\frac{\gamma}{\gamma - 1}) - \frac{1}{2}(p_s - p_\infty)} \tag{A11}$$

Using this result, equation (A9) can be solved for the shock velocity V_s

$$V_s = (V_n)_\infty - \left(\frac{p_s - p_\infty}{1 - \frac{1}{\rho_s}} \right)^{\frac{1}{2}} \tag{A12}$$

Using equation (A4), $(V_n)_s$ is obtained

$$(V_n)_s = \frac{1}{\rho_s}[(V_n)_\infty - V_s] + V_s \tag{A13}$$

Thus the components of velocity downstream of the shock wave are simply

$$(v_r)_s = -(V_n)_s \cos\zeta_s + V_\infty \cos\beta_s \sin\zeta_s \tag{A14}$$

$$(v_\phi)_s = (V_n)_s \sin\zeta_s + V_\infty \cos\beta_s \sin\zeta_s \qquad \text{(A15)}$$

For CF_4 or equilibrium air chemistry, the γ appearing in equation (A11) is replaced by γ_ρ. This allows the same shock wave routines to be used for these gases as for an ideal gas. Although this approach is inconsistent in the transient sense, it becomes more and more exact as the steady-state solution is approached. It also reduces the amount of work required to obtain converged solutions for these cases.

REFERENCES

1. Hayes, Wallace D. and Probstein, Ronald F.: Hypersonic Flow Theory. Volume I - Inviscid Flows. Second ed., Academic Press, Inc., 1966.

2. Van Dyke, Milton D. and Gordon, Hellen D.: Supersonic Flow Past a Family of Blunt Axisymmetric Bodies. NASA TR R-1, 1959.

3. Fuller, Franklyn B.: Numerical Solutions for Supersonic Flow of an Ideal Gas Around Blunt Two-Dimensional Bodies. NASA TN D-791, 1961.

4. Lomax, Harvard and Inouye, Mamoru: Numerical Analysis of Flow Properties About Blunt Bodies Moving at Supersonic Speeds in Equilibrium Gas. NASA TR R-204, 1964.

5. Hamilton, H. Harris II: Solution of Axisymmetric and Two-Dimensional Inviscid Flow Over Blunt Bodies by the Method of Lines. NASA TP 1154, 1978.

6. Moretti, Gino and Abbett, Michael: A Time-Dependent Computational Method for Blunt Body Flows. AIAA J., vol. 4, no. 12, Dec. 1966, pp. 2136-2141.

7. Barnwell, Richard W.: A Time-Dependent Method for Calculating Supersonic Blunt-Body Flow Fields With Sharp Corners and Embedded Shock Waves. NASA TN D-6031, 1970.

8. Moretti, Gino and Bleich, Gary: Three-Dimensional Flow Around Blunt Bodies. AIAA J., vol. 5, no. 9, Sept. 1967, pp. 1557-1562.

9. Barnwell, Richard W.: Three-Dimensional Method for Calculating Supersonic Angle-of-Attack Flow About Axisymmetric Blunt Bodies With Sharp Shoulders and Smooth Nonaxisymmetric Blunt Bodies. NASA TN D-6283, 1971.

10. Hamilton, H. Harris, II and Graves, Randolph A., Jr.: Application of a Numerically Generated Orthogonal Coordinate System to the Solution of Inviscid Axisymmetric Supersonic Flow Over Blunt Bodies. NASA TP 1619, 1980.

11. Weilmuenster, K. James and Hamilton, H. Harris, II: Calculations of Inviscid Flow Over Shuttle-Like Vehicles at High Angles of Attack and Comparisons With Experimental Data. NASA TP 2103, 1983.

12. Brailovskya, I. Yu.: A Difference Scheme for Numerical Solution of the Two-Dimensional, Nonstationary Navier-Stokes Equations for a Compressible Gas. Sov. Phys. - Doklady, vol. 10, no. 2, Aug. 1965, pp. 107-110.

13. Carter, James E.: Numerical Solutions of the Navier-Stokes Equations for the Supersonic Laminar Flow Over a Two-Dimensional Compression Corner. NASA TR R-385, 1972.

14. Sutton, Kenneth: Relations for the Thermodynamic and Transport Properties in the Testing Environment of the Langley Hypersonic CF_4 Tunnel. NASA TM 83220, 1981.

15. Hansen, C. Frederick: Approximations for the Thermodynamic and Transport Properties of High-Temperature Air. NASA TR R-50, 1959.

16. Belotserkovsky, O. M., ed.: Supersonic Gas Flow Around Blunt Bodies - Theoretical and Experimental Investigations. NASA TT F-453, 1967.

17. Sutton, Kenneth: Characteristics of Coupled Nongray Radiating Flows With Ablation Product Effects About Blunt Bodies During Planetary Entries. Ph.D. Thesis, North Carolina State Univ., 1973. (Available as NASA TM X-72078.)

18. Inouye, Mamoru; Rakich, John V.; and Lomax, Harvard: A Description of Numerical Methods and Computer Programs for Two-Dimensional and Axisymmetric Supersonic Flow Over Blunt-Nosed and Flared Bodies. NASA Technical Note, NASA TN D-2970, 1965.

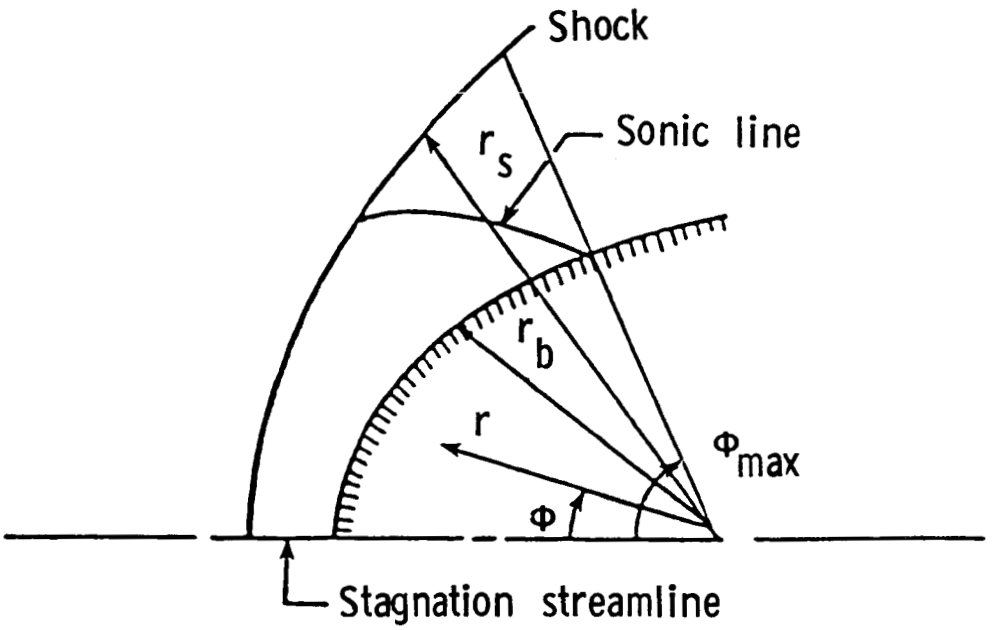

Figure 1. - Polar coordinate system.

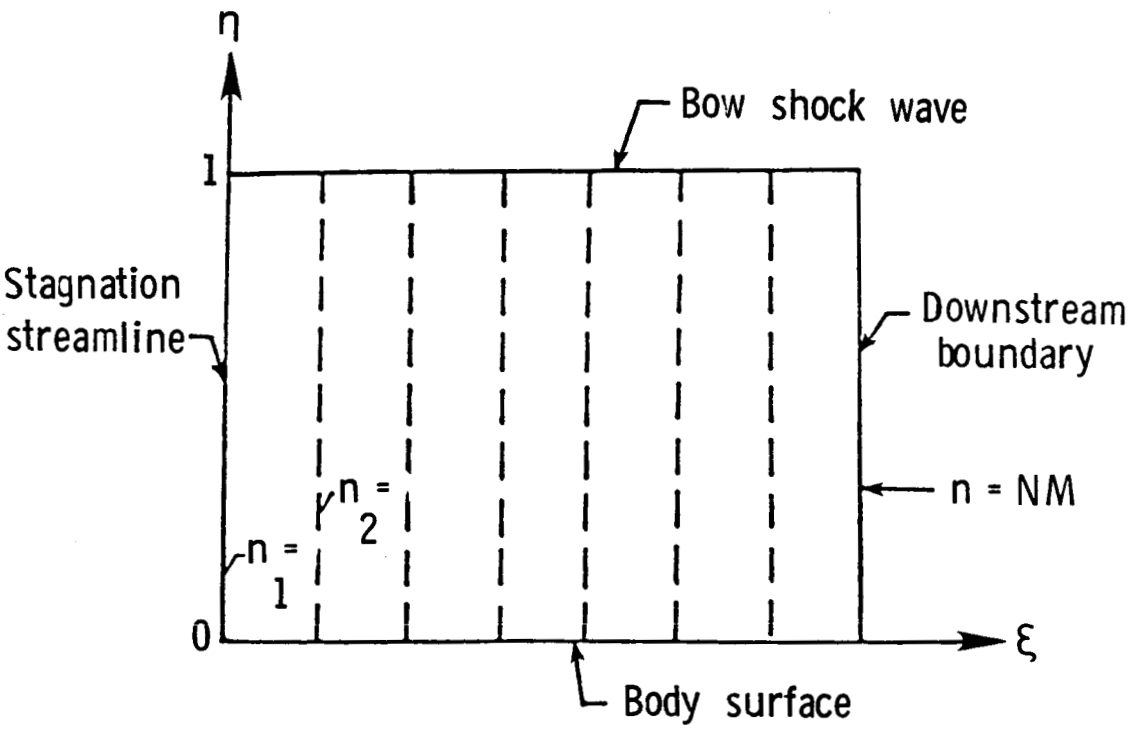

Figure 2. - Computational domain.

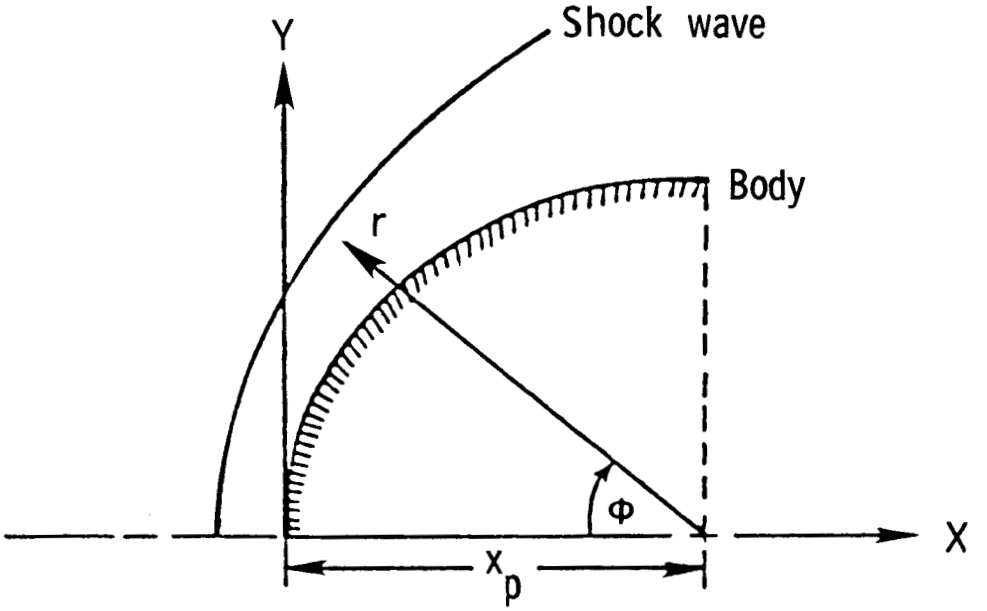

Figure 3. - Cartesian coordinate system.

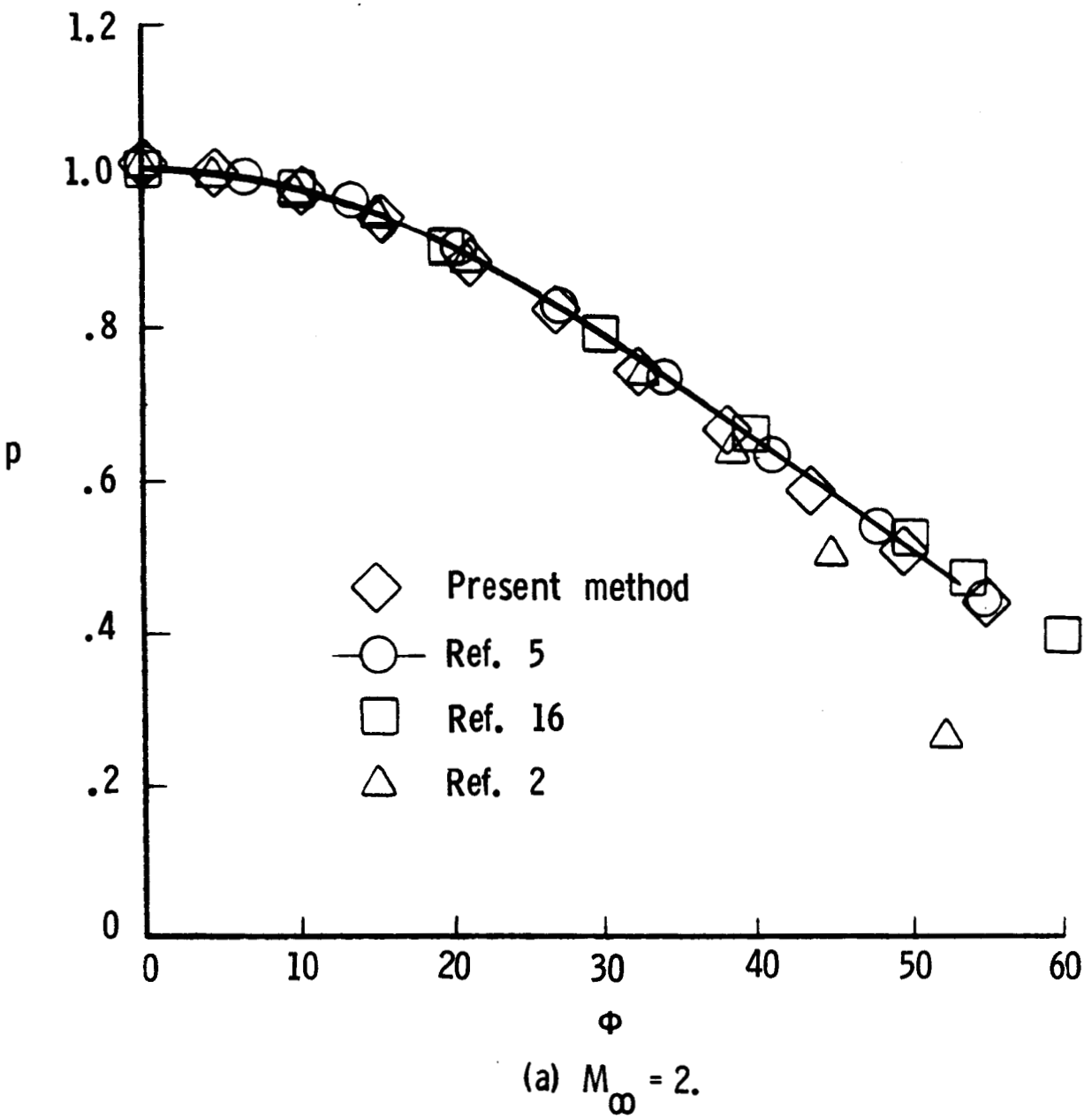

(a) $M_\infty = 2.$

Figure 4. - Pressure distribution on a sphere in air. Ideal gas with $\gamma = 1.4$.

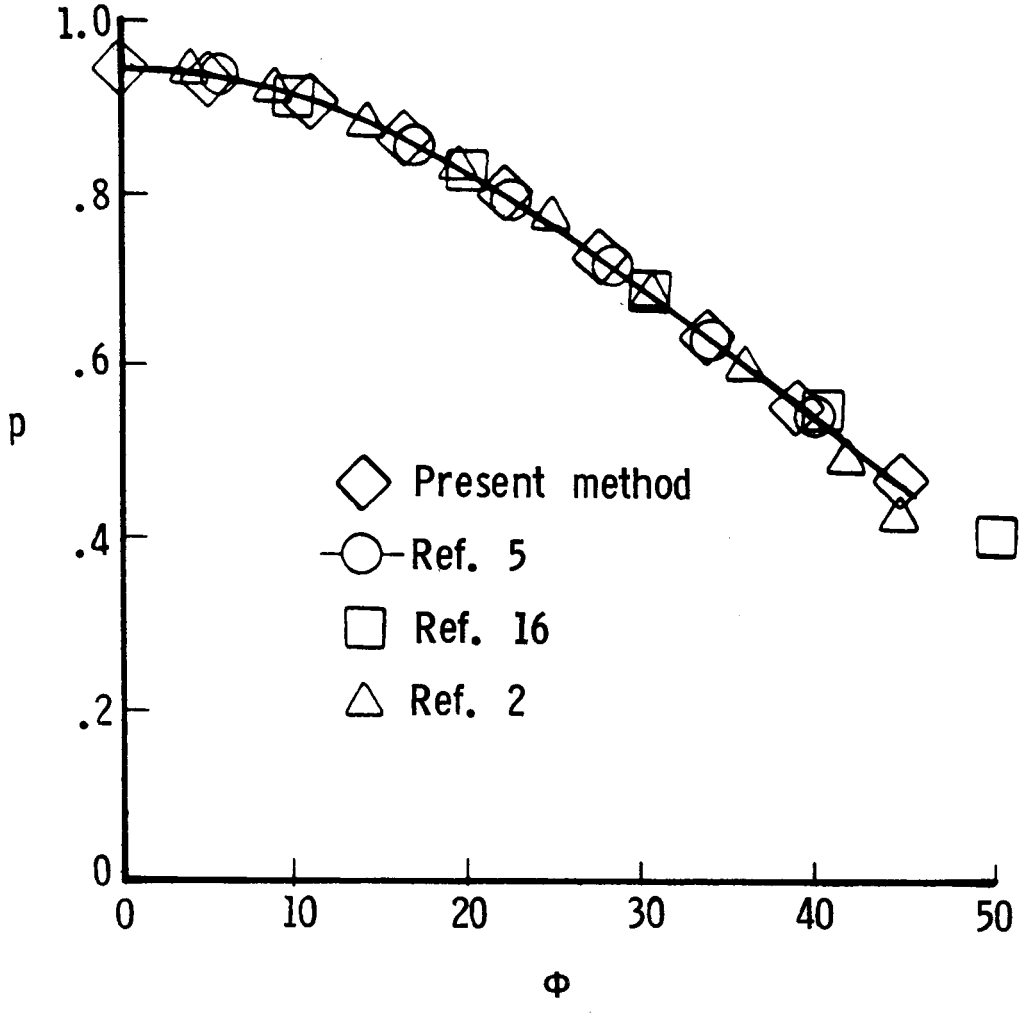

(b) $M_\infty = 4.$

Figure 4. - Continued.

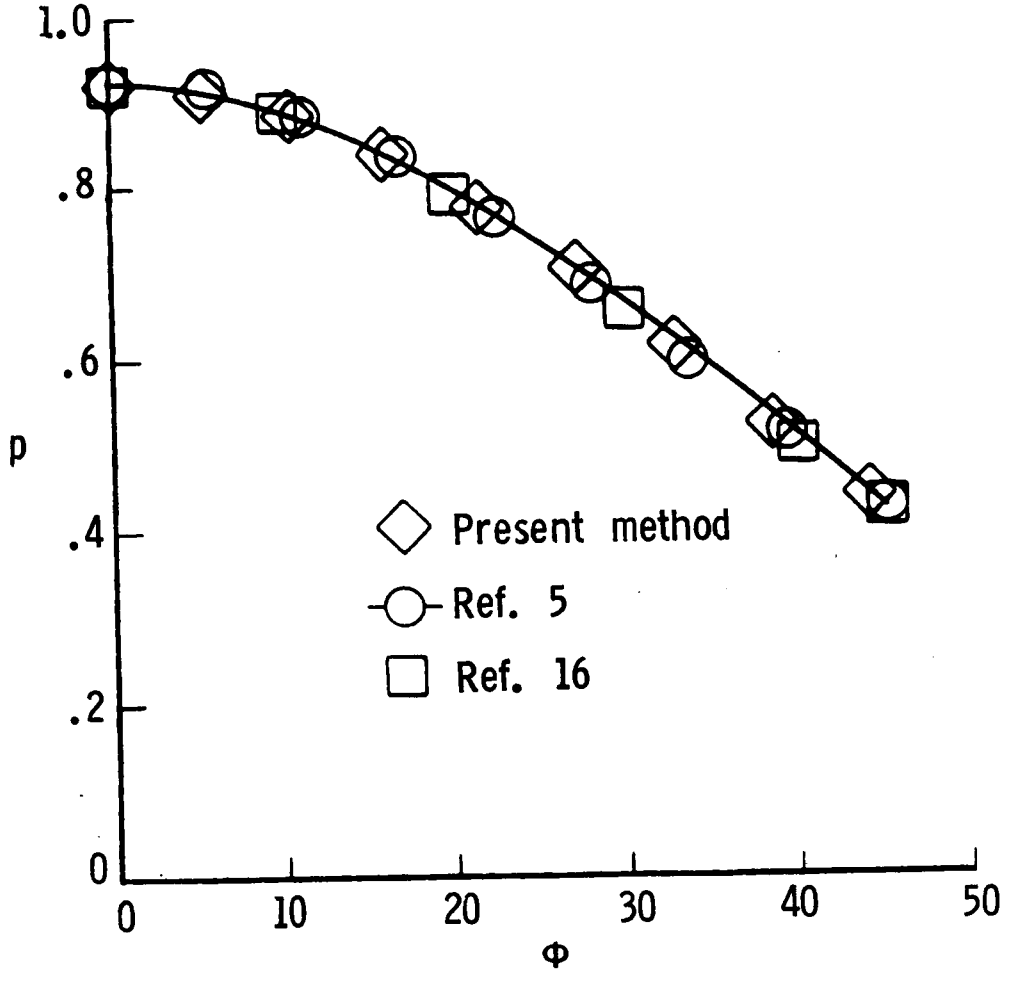

(c) $M_\infty = 8.06$.

Figure 4. - Concluded.

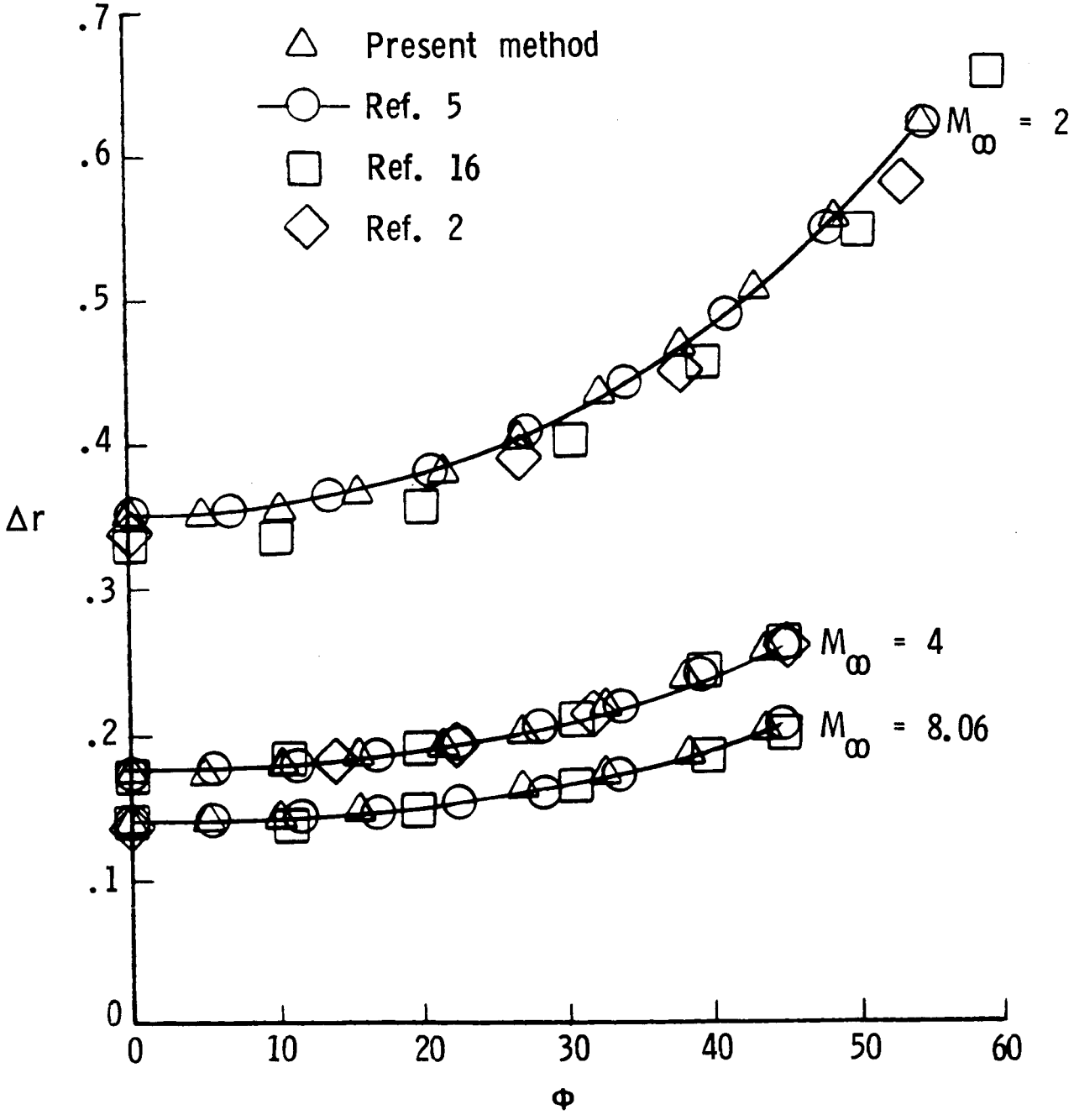

Figure 5. - Shock-layer thicknesses for a sphere in air. Ideal gas with $\gamma = 1.4$.

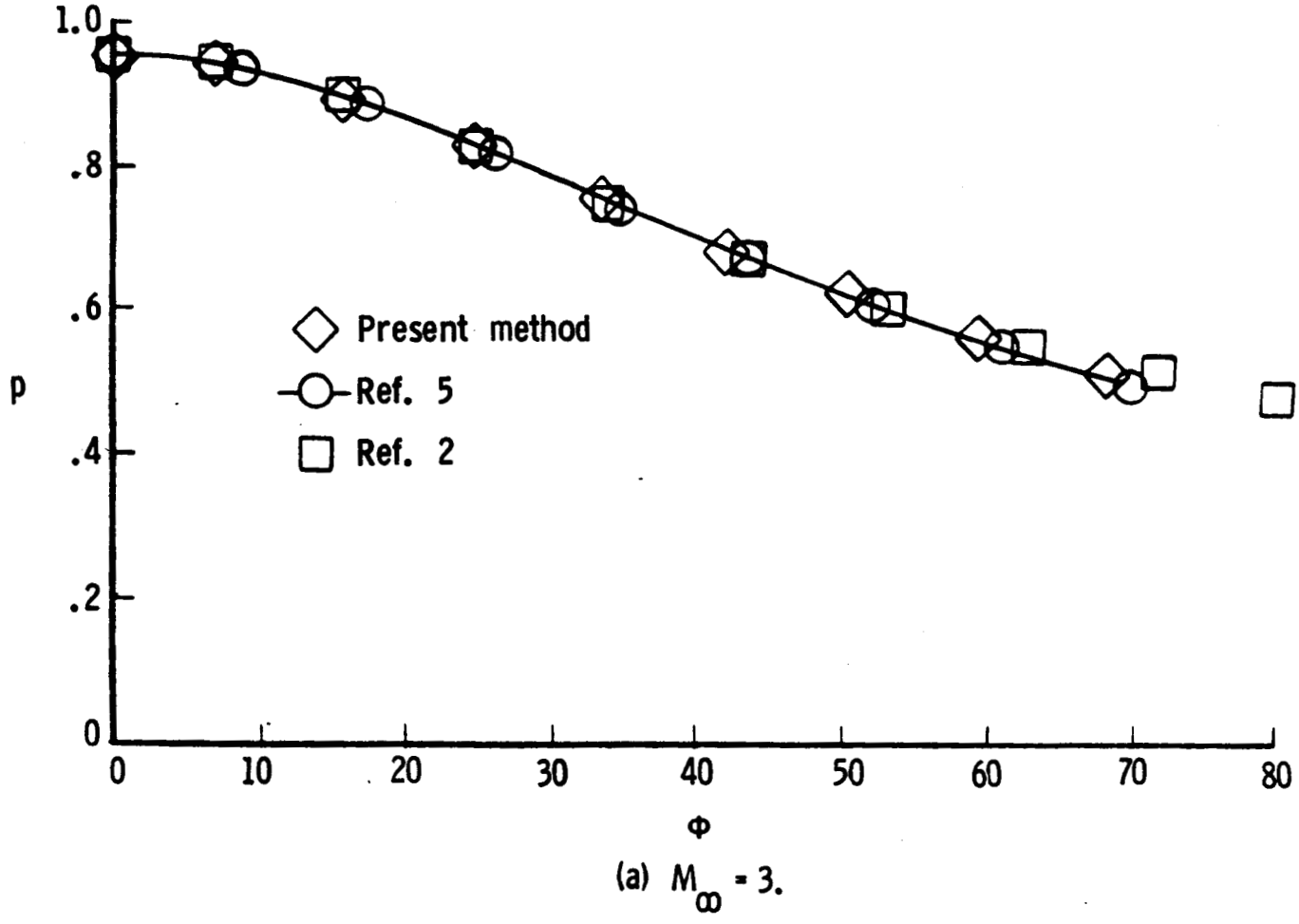

(a) $M_\infty = 3.$

Figure 6. - Pressure distribution on a paraboloid in air. Ideal gas with $\gamma = 1.4$.

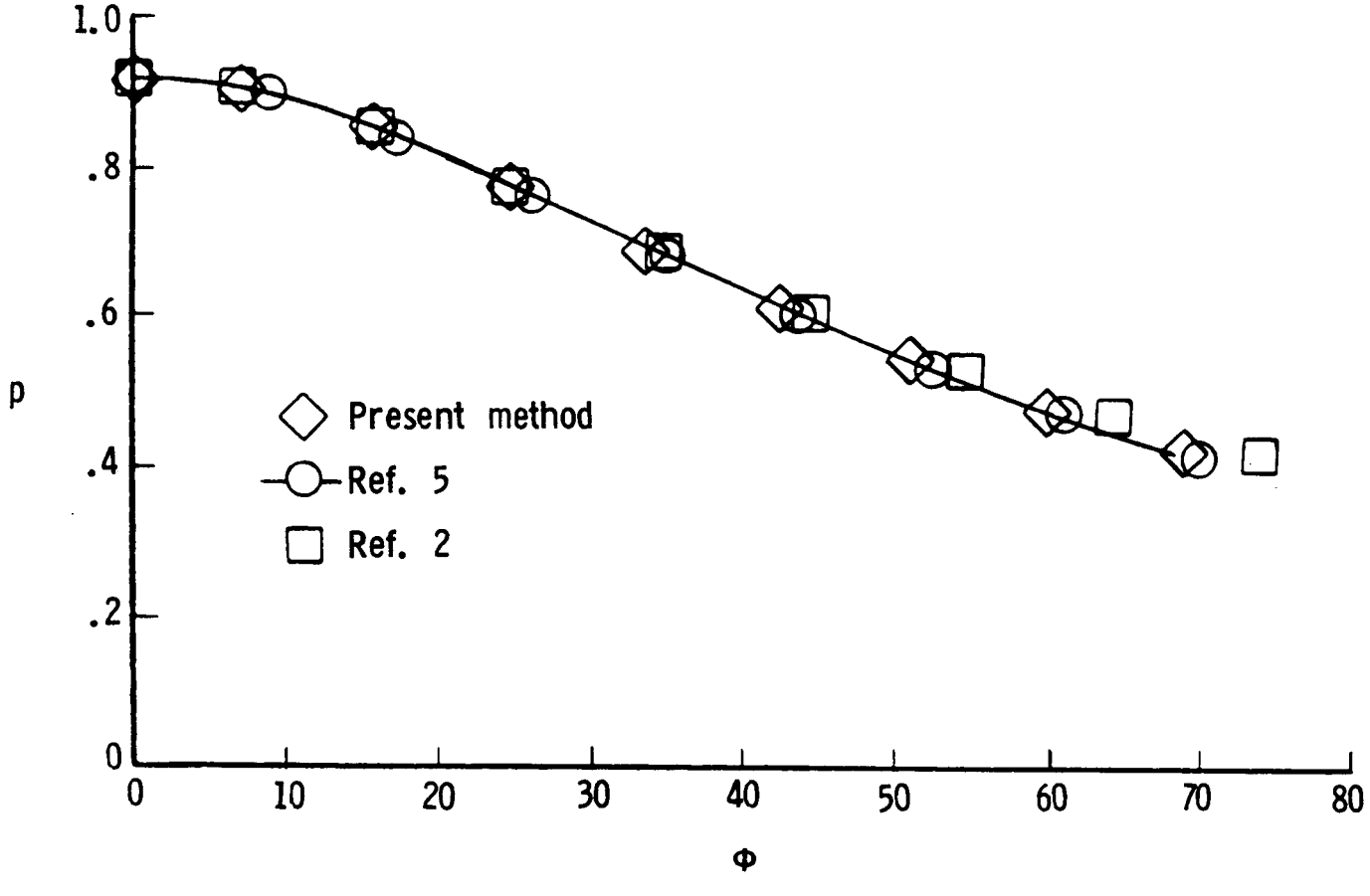

(b) $M_\infty = 10.$

Figure 6. - Concluded.

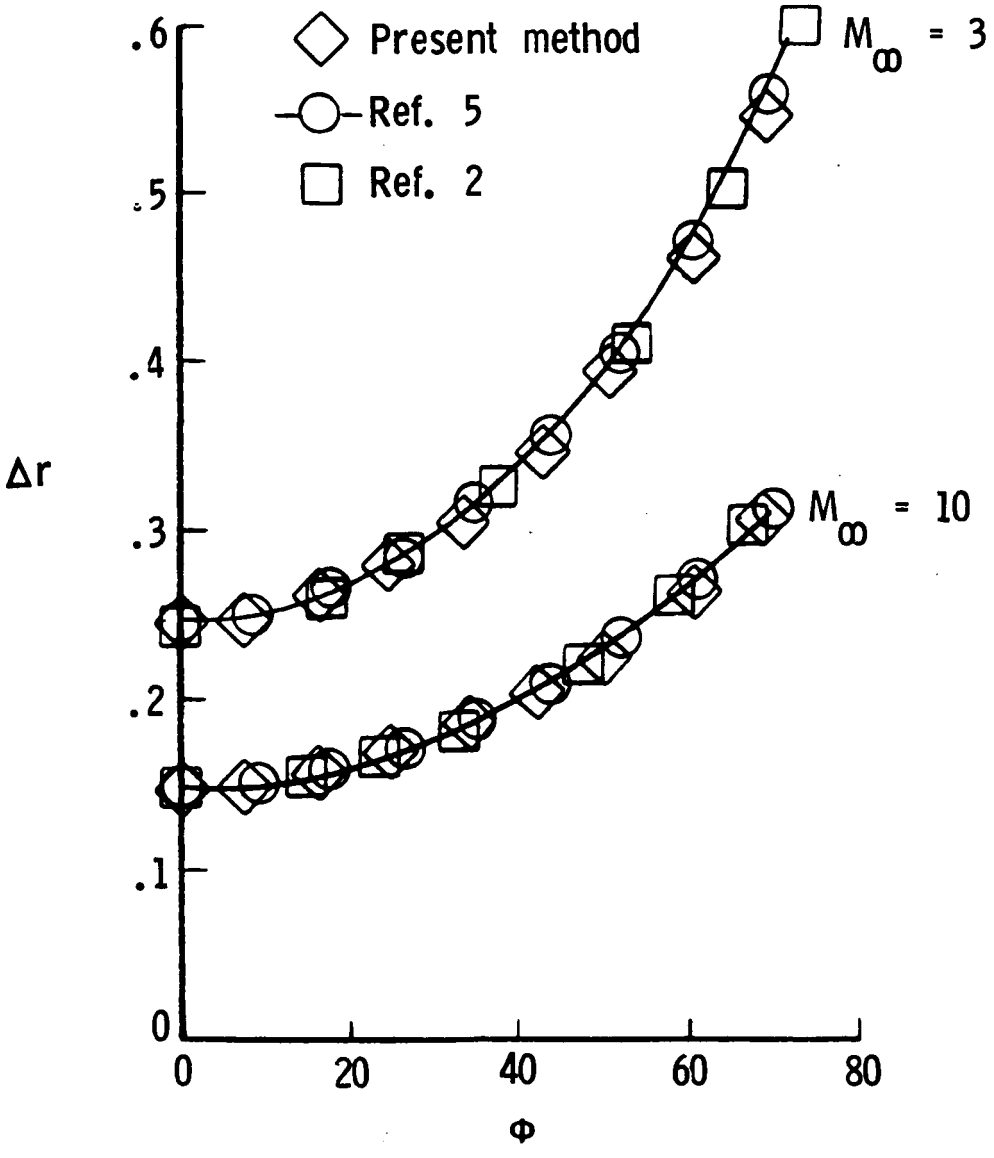

Figure 7. - Shock-layer thicknesses for a paraboloid in air. Ideal gas with $\gamma = 1.4$.

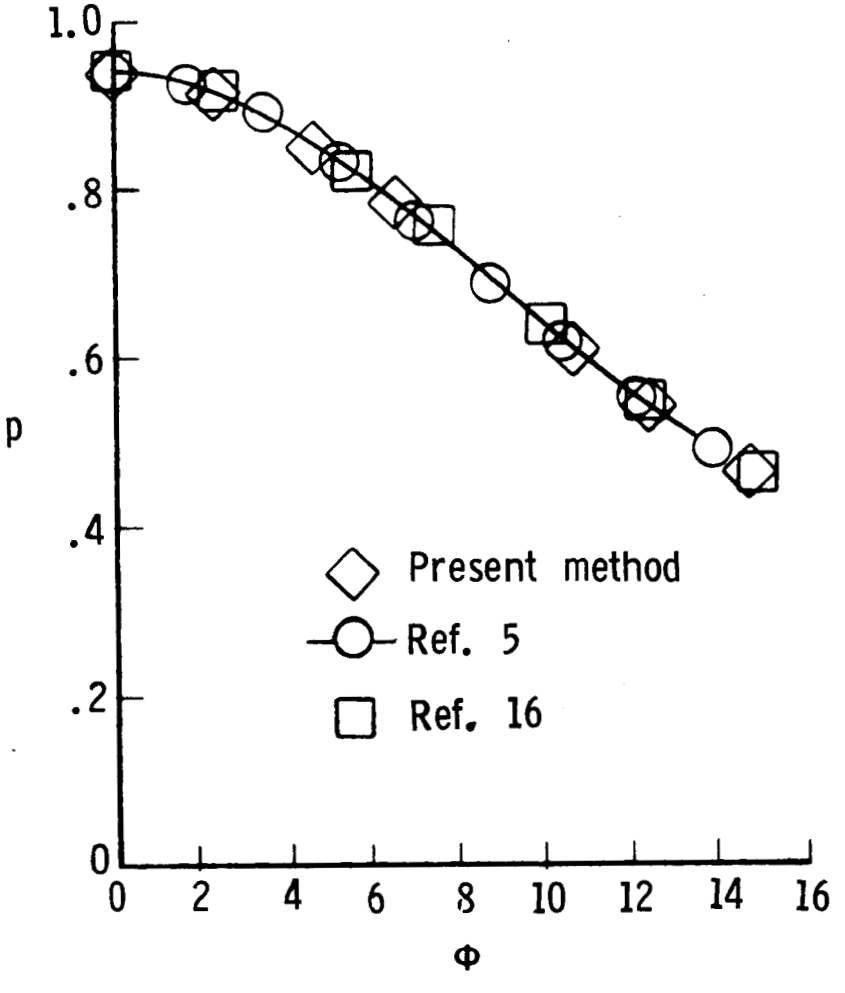

(a) $M_\infty = 4.$

Figure 8. - Pressure distribution on an ellipsoid in air. Ideal gas with $\gamma = 1.4$ and $b/a = 0.5$.

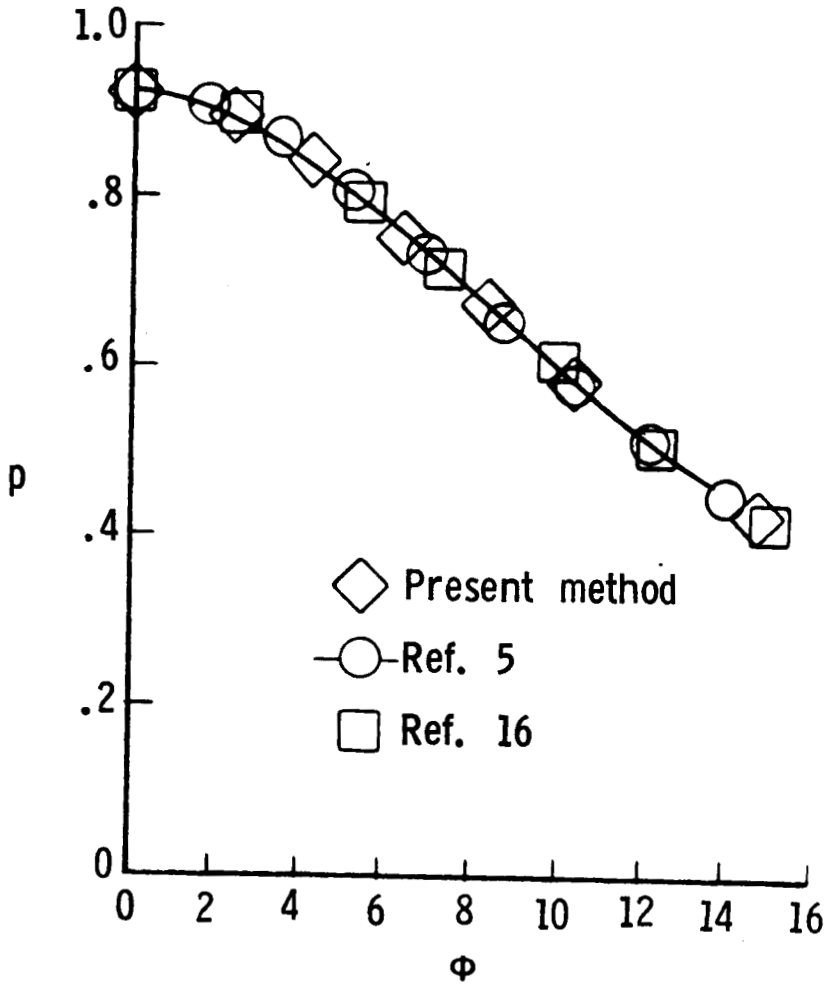

(b) $M_{\infty} = 8.06$.

Figure 8. - Concluded.

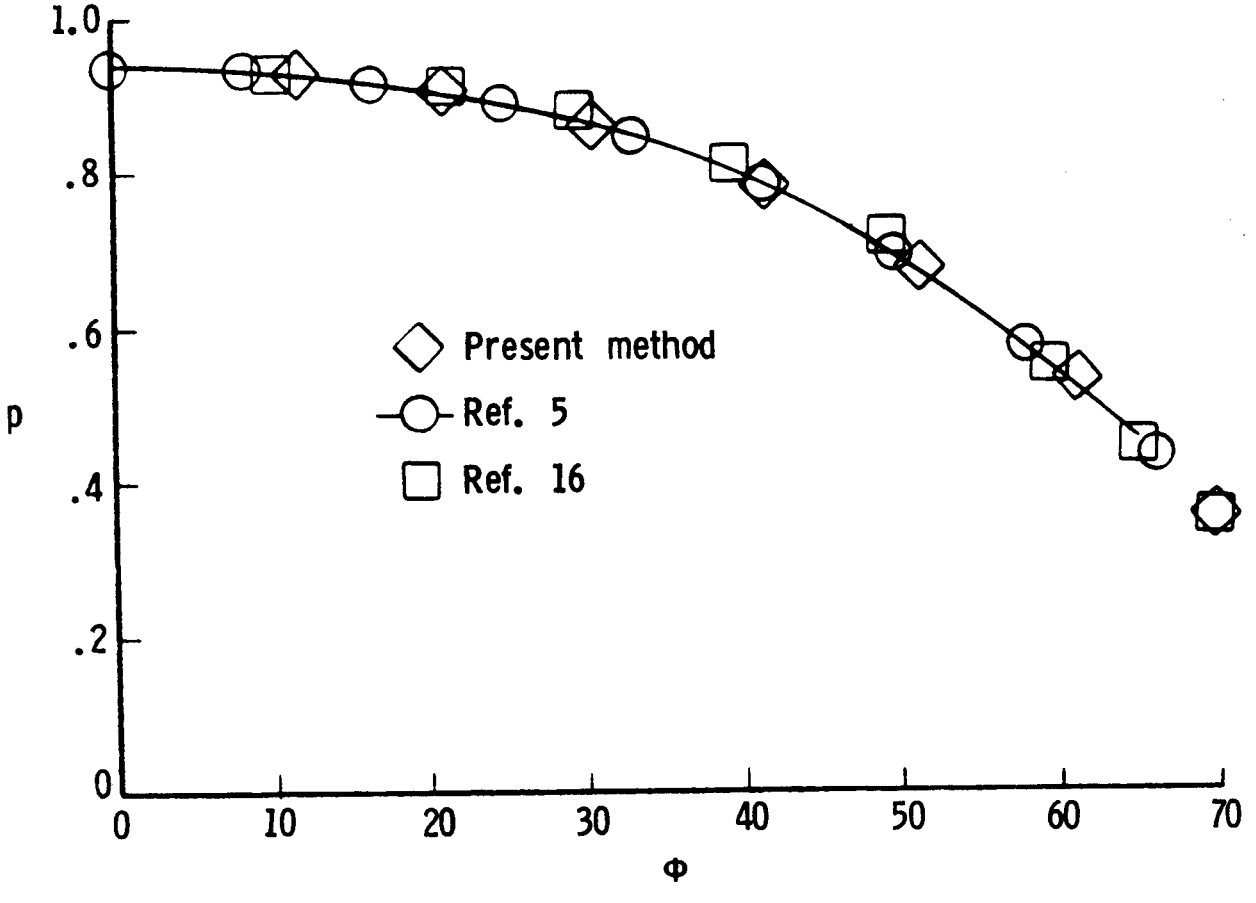

(a) $M_\infty = 4.$

Figure 9. - Pressure distribution on an ellipsoid in air. Ideal gas with $\gamma = 1.4$. and $b/a = 1.5$.

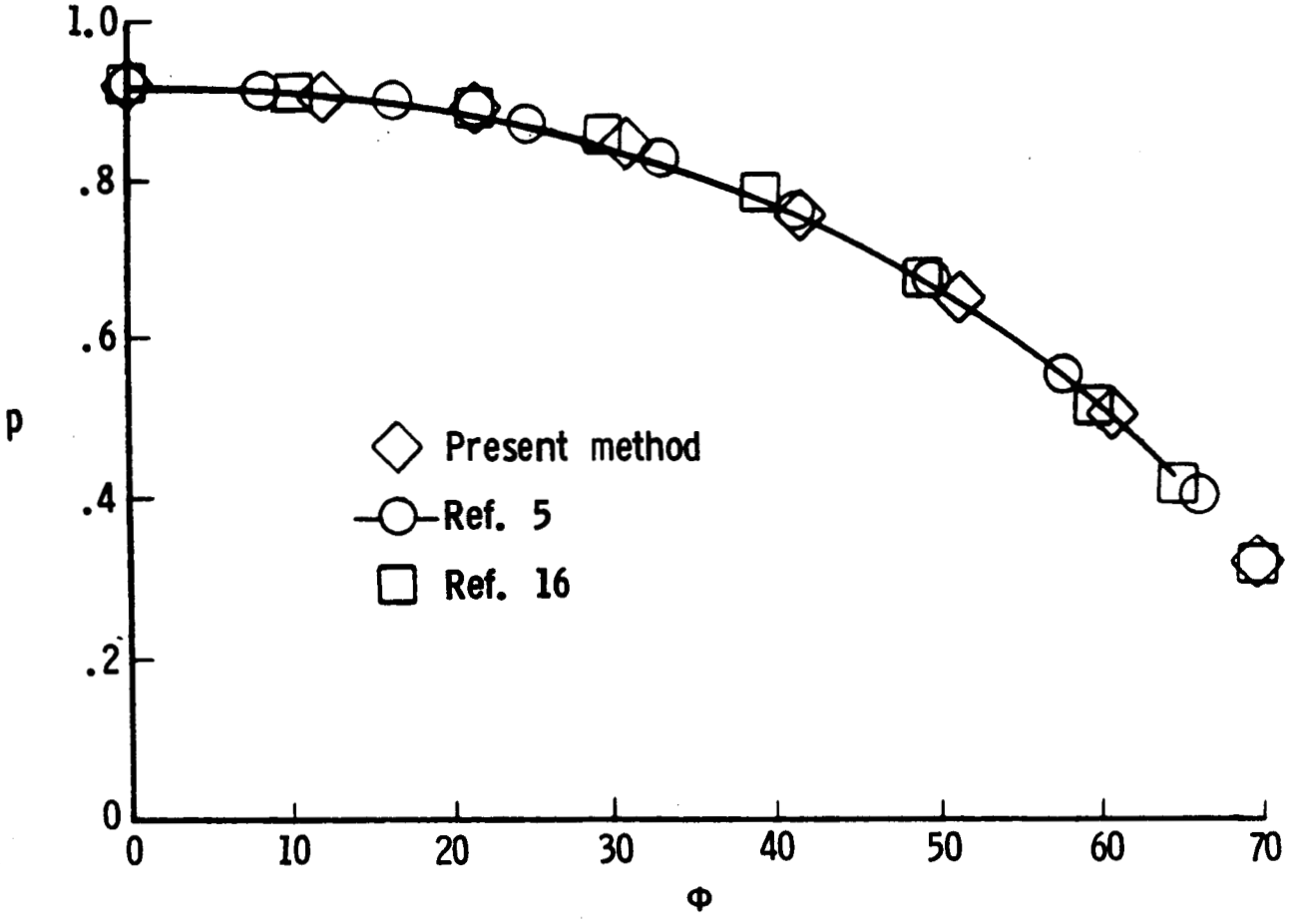

(b) $M_\infty = 8.06$.

Figure 9. - Concluded.

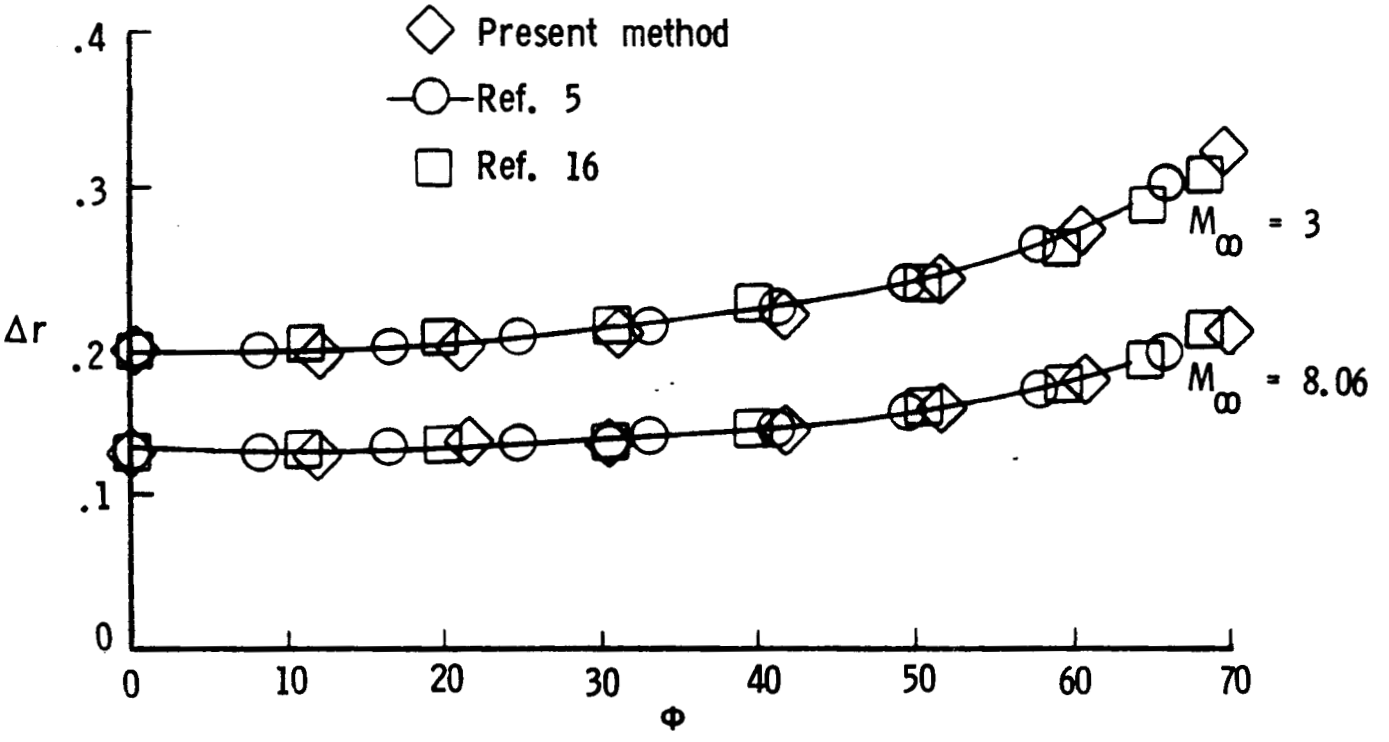

Figure 10. - Shock-layer thicknesses for an ellipsoid in air. Ideal gas with $\gamma = 1.4$ and $b/a = 1.5$.

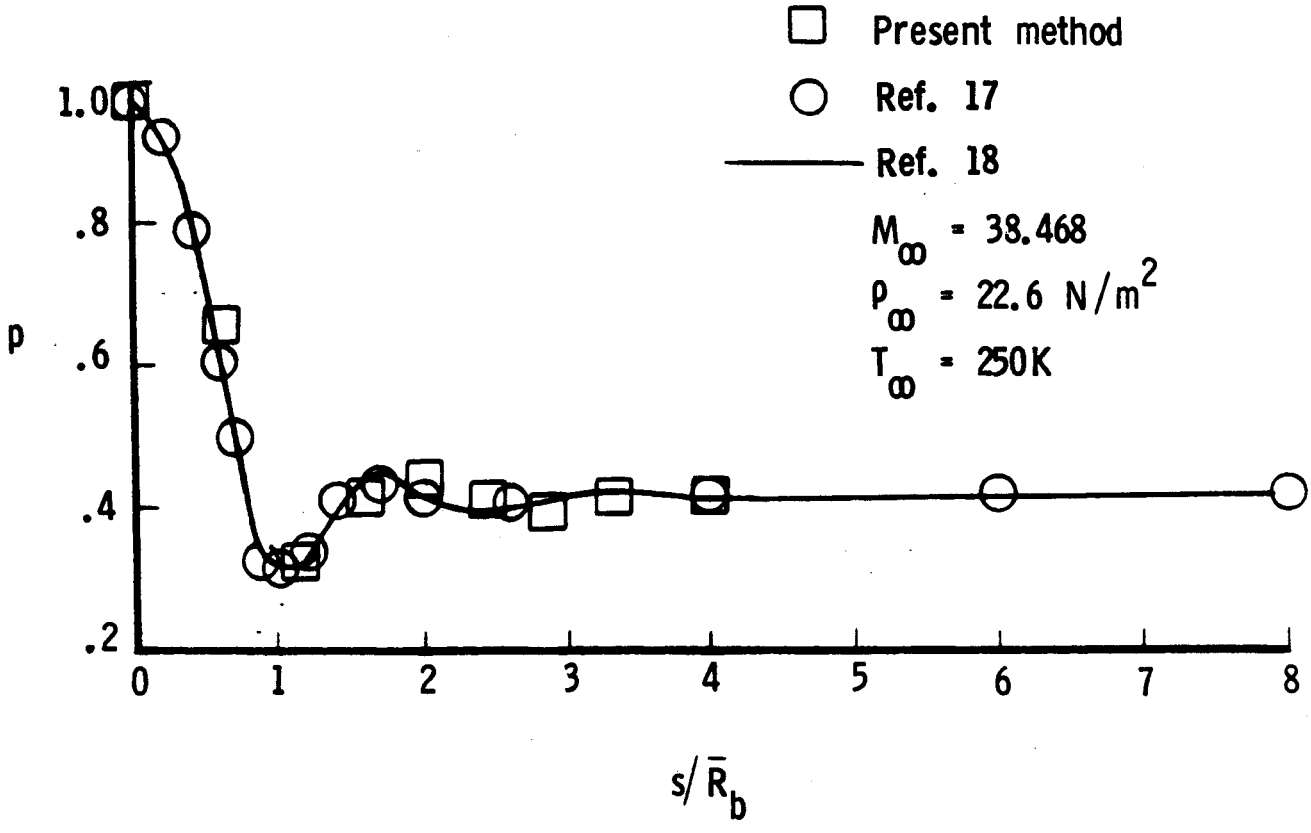

Figure 11. - Pressure distribution on a 40° sphere-cone in air with equilibrium chemistry.

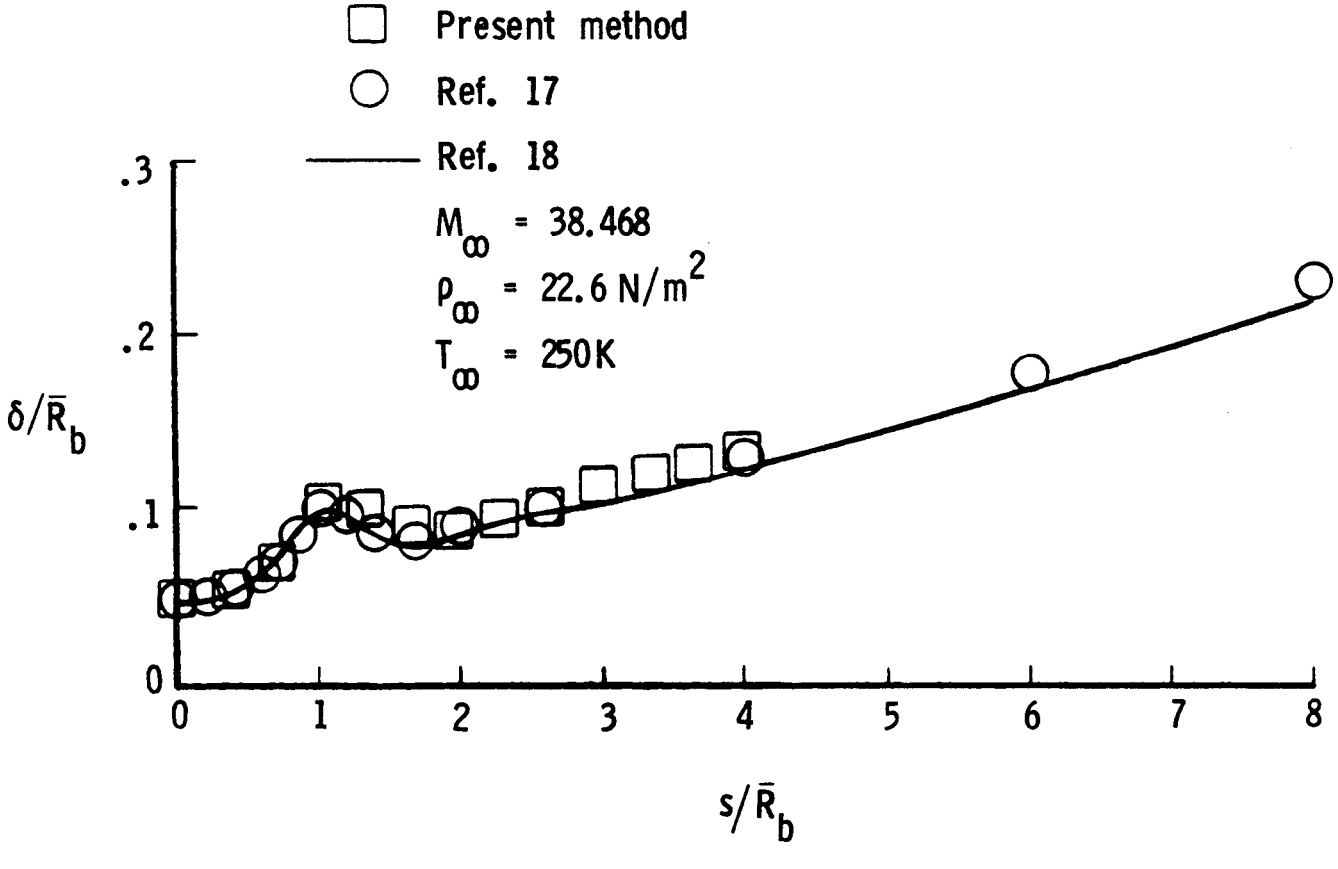

Figure 12. - Shock stand-off distance for a 40° sphere-cone in air with equilibrium chemistry.

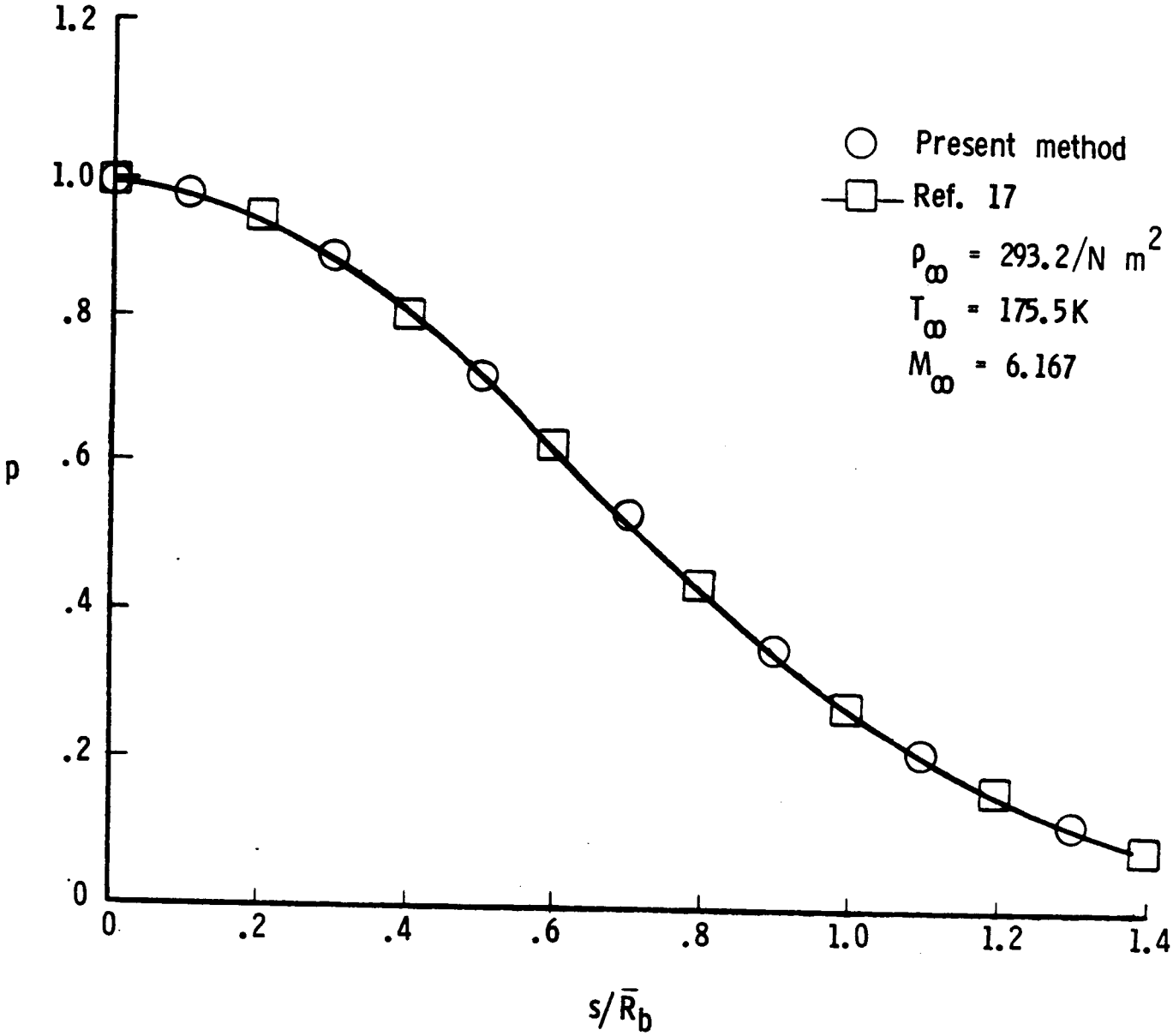

Figure 13. - Pressure distribution on a sphere in CF_4.

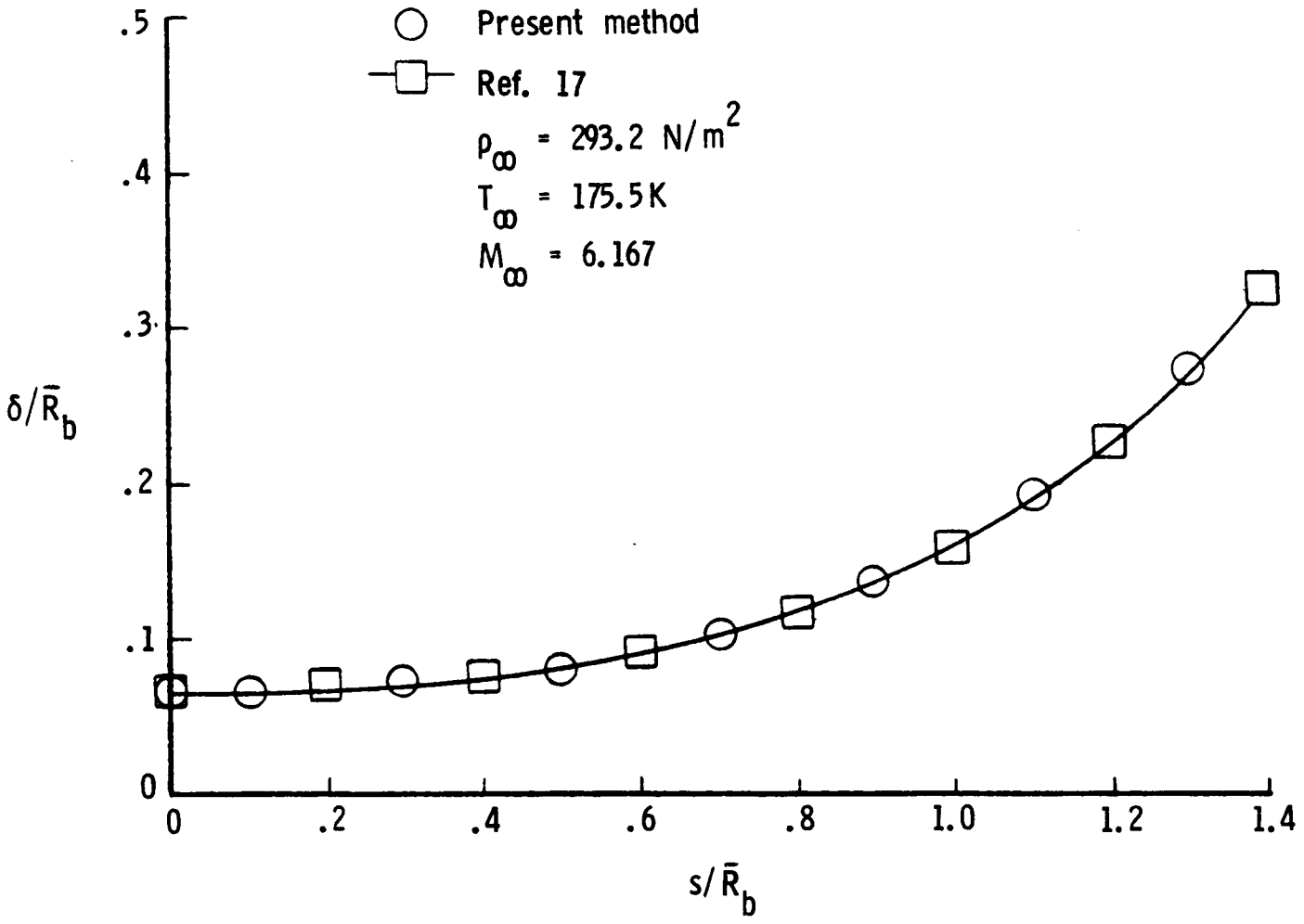

Figure 14. - Shock-layer thicknesses for a sphere in CF_4.

1. Report No.	2. Government Accession No.	3. Recipient's Catalog No.
NASA TM-87675		

4. Title and Subtitle	5. Report Date
Time-Dependent Solution for Axisymmetric Flow Over a Blunt Body with Ideal Gas, CF_4, or Equilibrium Air Chemistry	July 1986
	6. Performing Organization Code: 506-40-11-02
7. Author(s): H. Harris Hamilton II, John R. Spall	8. Performing Organization Report No.
	10. Work Unit No.
9. Performing Organization Name and Address: Langley Research Center, Hampton, Virginia 23665	11. Contract or Grant No.
	13. Type of Report and Period Covered: Technical Memorandum
12. Sponsoring Agency Name and Address: National Aeronautics and Space Administration, Washington, DC 20546	14. Sponsoring Agency Code

15. Supplementary Notes

16. Abstract

A time-asymptotic method has been used to obtain steady-flow solutions for axisymmetric inviscid flow over several blunt bodies including spheres, paraboloids, ellipsoids, and spherically blunted cones. Comparisons with experimental data and results of other computational methods have demonstrated that accurate solutions can be obtained using this approach. The method should prove useful as an analysis tool for comparing with experimental data and for making engineering calculations for blunt reentry vehicles.

17. Key Words (Suggested by Author(s))	18. Distribution Statement
Blunt Body Inviscid Flow Field Time Dependent	Unclassified - Unlimited Subject Category 34

19. Security Classif. (of this report)	20. Security Classif. (of this page)	21. No. of Pages	22. Price
unclassified	unclassified	39	A03

For sale by the National Technical Information Service, Springfield, Virginia 22161